Turing pattern selection in a reaction–diffusion epidemic model*

Wang Wei-Ming(王玮明)[a)†], Liu Hou-Ye(刘厚业)[a)], Cai Yong-Li (蔡永丽)[a)], and Li Zhen-Qing (李镇清)[b)]

[a)] *College of Mathematics and Information Science, Wenzhou University, Wenzhou* 325035, *China*

[b)] *State Key Laboratory of Vegetation and Environmental Change, Institute of Botany, Chinese Academy of Sciences, Beijing* 100093, *China*

(Received 8 January 2011; revised manuscript received 25 February 2011)

We present Turing pattern selection in a reaction–diffusion epidemic model under zero-flux boundary conditions. The value of this study is twofold. First, it establishes the amplitude equations for the excited modes, which determines the stability of amplitudes towards uniform and inhomogeneous perturbations. Second, it illustrates all five categories of Turing patterns close to the onset of Turing bifurcation via numerical simulations which indicates that the model dynamics exhibits complex pattern replication: on increasing the control parameter ν, the sequence "H_0 hexagons $\rightarrow$ H_0-hexagon-stripe mixtures $\rightarrow$ stripes $\rightarrow$ H_π-hexagon-stripe mixtures $\rightarrow$ H_π hexagons" is observed. This may enrich the pattern dynamics in a diffusive epidemic model.

Keywords: epidemic model, pattern selection, amplitude equations, Turing instability

PACS: 47.54.–r, 87.23.Cc, 89.75.Kd **DOI:** 10.1088/1674-1056/20/7/074702

1. Introduction

In epidemiology, mathematical models have been an important method in analysing the spread and control of infectious diseases qualitatively and quantitatively. The research results are helpful to predict the developing tendency of the infectious diseases, to determine the key factors to the spread of them and to seek the optimum strategies of preventing and controlling the spreading of them.[1] Researches in theoretical and mathematical epidemiology have proposed many epidemic models to understand the mechanism of disease transmissions.[2−15]

More recently, many studies[16−38] have provided that spatial epidemic model is an appropriate tool for investigating fundamental mechanism of complex spatiotemporal epidemic dynamics. In these studies, reaction–diffusion equations have been intensively used to describe spatiotemporal dynamics, in which the spatial spreading of infectious is studied by analysing travelling wave solutions and calculating spreading rates.

Furthermore, there are some researches of pattern formation in the spatial epidemic model, starting with the pioneer work of Turing.[39] Turing's revolutionary idea was that the passive diffusion could interact with a chemical reaction in such a way that even if the reaction by itself has no symmetry-breaking capabilities, diffusion can de-stabilize the symmetric solutions so that the system with diffusion can have them.[21] Spatial epidemiology with diffusion has become a principal scientific discipline aiming at understanding the causes and consequences of spatial heterogeneity in infectious diseases.[24,33,36−38] In these studies, the authors investigated the pattern formation of a spatial epidemic model with self-diffusion or cross-diffusion and found that model dynamics exhibits a diffusion-controlled formation growth to stripes, spots and coexistence or chaos pattern replication. However, these studies only focus on the bifurcation phenomena when varying the controlling parameter(s), and little attention has been paid to the study on the selection of Turing patterns.

Due to the insightful work of many scientists over recent decades, we can now focus on pattern selection by using the standard multiple-scale analysis. The key of this method is the so-called amplitude equations.[40−54] The amplitude equations formalism introduced by Newell and Whitehead,[40] and Segel[44] is a natural scheme to extract universal properties of

*Project supported by the Natural Science Foundation of Zhejiang Province of China (Grant No. Y7080041).

†Corresponding author. E-mail: weimingwang2003@163.com

© 2011 Chinese Physical Society and IOP Publishing Ltd

pattern formation. Amplitude equations describe slow modulations in space and time of a simple basic pattern that can be determined from the linear analysis of the equations of motion of the reaction–diffusion system. Amplitude equations have been discussed in some reaction–diffusion systems.[42,49,52−54]

Based on the discussion above, in this paper, we focus mainly on the Turing pattern selection in a spatial epidemic model. The organization of this paper is as follows. In the next section, we introduce the two-dimensional epidemic model and give a general survey of the linear stability analysis and bifurcations with zero-flux boundary conditions. In Section 3, we carry out the multiple-scale analysis to derive the amplitude equations and present and discuss the results of Turing pattern formation via numerical simulation, too. Finally, conclusions and remarks are presented in Section 4.

2. The model and Turing instability analysis

2.1. The model system

In Ref. [7], Berezovsky and co-workers introduced a simple epidemic model. The total population (N) is divided into two groups susceptible (S) and infectious (I), i.e., $N = S + I$. The model describing the relations between the state variables is

$$\begin{aligned}\frac{\mathrm{d}S}{\mathrm{d}t} &= rN\left(1-\frac{N}{K}\right)-\beta\frac{SI}{N}-(\mu+m)S,\\ \frac{\mathrm{d}I}{\mathrm{d}t} &= \beta\frac{SI}{N}-(\mu+d)I,\end{aligned} \tag{1}$$

where the birth process incorporates density dependent effects via a logistic equation with the intrinsic growth rate r and the carrying capacity K, β denotes the transmission rate (the infection rate is constant), μ is the natural mortality; d denotes the disease-induced mortality and m is the per-capita emigration rate of uninfective.

The concept of basic demographic reproductive number R_d is given by

$$R_\mathrm{d} = \frac{r}{\mu+m}.$$

It can be shown that if $R_\mathrm{d} > 1$, the population grows, while $R_\mathrm{d} < 1$ implies that the population does not survive.

The epidemic threshold, the basic reproductive number, is then computed as

$$R_0 = \frac{\beta}{\mu+d}.$$

Usually, the disease will successfully invade when $R_0 > 1$ but will die out if $R_0 < 1$.

Re-scalling the model (1) by letting

$$S \to S/K, \quad I \to I/K, \quad t \to t/(\mu+d)$$

leads to the following model:

$$\begin{aligned}\frac{\mathrm{d}S}{\mathrm{d}t} &= \nu R_\mathrm{d}(S+I)(1-(S+I)\,)-R_0\frac{SI}{S+I}-\nu S,\\ \frac{\mathrm{d}I}{\mathrm{d}t} &= R_0\frac{SI}{S+I}-I,\end{aligned} \tag{2}$$

where $\nu = (\mu+m)/(\mu+d)$ is the ratio of the average life-span of susceptible to that of infectious.

For details, we refer to the reader Section 2 in Ref. [7].

For simplicity, skip the term $-\nu S$ in the first expression of Eq. (2), and by a change of independent variable $\mathrm{d}t \to (S+I)\mathrm{d}t$, we can obtain the modified model in the first quadrant that is equivalent to the polynomial system

$$\begin{aligned}\frac{\mathrm{d}S}{\mathrm{d}t} &= \nu R_\mathrm{d}(S+I)^2(1-(S+I)\,)-R_0SI,\\ \frac{\mathrm{d}I}{\mathrm{d}t} &= R_0SI-I(S+I).\end{aligned} \tag{3}$$

Assume that the susceptible (S) and infectious (I) population move randomly, described as Brownian random motion, then we propose a simple spatial model corresponding to Eq. (3) as follows:

$$\begin{aligned}\frac{\partial S}{\partial t} &= \nu R_\mathrm{d}(S+I)^2(1-(S+I)\,)-R_0SI+d_1\boldsymbol{\nabla}^2S\\ &= f(S,I)+d_1\boldsymbol{\nabla}^2S,\\ \frac{\partial I}{\partial t} &= R_0SI-I(S+I)+d_2\boldsymbol{\nabla}^2I = g(S,I)+d_2\boldsymbol{\nabla}^2I,\end{aligned} \tag{4}$$

where the nonnegative constants d_1 and d_2 are the diffusion coefficients of S and I, respectively. $\boldsymbol{\nabla}^2 = \frac{\partial^2}{\partial x^2}+\frac{\partial^2}{\partial y^2}$, the usual Laplacian operator in two-dimensional space, is used to describe the Brownian random motion.[55]

Model (4) is to be analysed under the following non-zero initial condition:

$$\begin{aligned}&S(\boldsymbol{r},0)>0, \quad I(\boldsymbol{r},0)>0,\\ &\boldsymbol{r}=(x,y)\in\Omega=[0,L]\times[0,L],\end{aligned} \tag{5}$$

and zero-flux boundary condition

$$\frac{\partial S}{\partial n} = \frac{\partial I}{\partial n} = 0. \tag{6}$$

In the above Eqs. (5) and (6), L denotes the size of the system in the directions of x and y; n is the outward unit normal vector of the boundary $\partial\Omega$. The main reason for choosing such boundary conditions is that we are interested in the self-organization of patterns. And zero-flux conditions imply that there is no flux of population through the boundary, i.e., no external input is imposed from outside.[56]

In the absence of diffusion, considering model (1), model (4) has one disease-free equilibrium $E_1 = (1, 0)$, which corresponds to the susceptible population being at its carrying capacity with no infected population and an endemic equilibrium point $E^* = (S^*, I^*)$, which depends on the parameters R_d and R_0 and ν is given implicitly by

$$S^* = \frac{\nu R_0 R_\mathrm{d} - R_0 + 1}{\nu R_0^2 R_\mathrm{d}}, \quad I^* = (R_0 - 1)S^*. \tag{7}$$

It is easy to see that $S^* > 0, I^* > 0$ when

$$1 < R_0 < \frac{1}{1 - \nu R_\mathrm{d}}. \tag{8}$$

In the presence of diffusion, we set $S = S^* + \widetilde{S}$, $I = I^* + \widetilde{I}$, where $\widetilde{S}$, $\widetilde{I} \ll 1$. For simplicity, we still write $\widetilde{S}$, $\widetilde{I}$ as S, I and linearize Eq. (4) in S and I to obtain

$$\begin{aligned} \frac{\partial S}{\partial t} &= f_S S + f_I I + d_1 \boldsymbol{\nabla}^2 S, \\ \frac{\partial I}{\partial t} &= g_S S + g_I I + d_2 \boldsymbol{\nabla}_2 I, \end{aligned} \tag{9}$$

where

$$\begin{aligned} f_S &= \left.\frac{\partial f}{\partial S}\right|_{(S^*, I^*)} = 2\nu R_\mathrm{d}(S^* + I^*)(1 - S^* - I^*) \\ &\quad - \nu R_\mathrm{d}(S^* + I^*)^2 - R_0 I^*, \\ f_I &= \left.\frac{\partial f}{\partial I}\right|_{(S^*, I^*)} = 2\nu R_\mathrm{d}(S^* + I^*)(1 - S^* - I^*) \\ &\quad - \nu R_\mathrm{d}(S^* + I^*)^2 - R_0 S^*, \\ g_S &= \left.\frac{\partial g}{\partial S}\right|_{(S^*, I^*)} = (R_0 - 1)I^*, \\ g_I &= \left.\frac{\partial g}{\partial I}\right|_{(S^*, I^*)} = (R_\mathrm{d} - 1)S^* - 2I^*. \end{aligned}$$

It is well known that the equilibrium $E^* = (S^*, I^*)$ of model (4) is stable if both eigenvalues are negative, with $f_S < g_I$ and $f_S g_I < f_I g_S$.

Any solution of model (9) can be expressed as a Fourier series in space,[49–53] which grow in the form

$$\begin{aligned} S(\boldsymbol{r}, t) &\sim \exp(\lambda t + \mathrm{i}\boldsymbol{k} \cdot \boldsymbol{r}), \\ I(\boldsymbol{r}, t) &\sim \exp(\lambda t + \mathrm{i}\boldsymbol{k} \cdot \boldsymbol{r}), \end{aligned} \tag{10}$$

where $\boldsymbol{k} \cdot \boldsymbol{k} = k^2$, k and λ are the wave-number and frequency, respectively.

Substituting the above equation into Eq. (9) leads to the dispersion relation for λ

$$\begin{aligned} &\lambda^2 - \left(f_S + g_I - (d_1 + d_2)k^2\right)\lambda + f_S g_I \\ &\quad - f_I g_S - k^2(f_S d_2 + g_I d_1) + k^4 d_1 d_2 = 0. \end{aligned} \tag{11}$$

2.2. Turing instability

We know that one type of instability (or bifurcation) will break the type of symmetry of a system, i.e., at the bifurcation point, two equilibrium states coexist and will exchange their stabilities. Biologically speaking, this bifurcation corresponds to a smooth transition between equilibrium states.[55–60]

The Turing instability, mathematically speaking, for $d_1 \ll d_2$, occurs when $\mathrm{Im}(\lambda(k)) = 0$, $\mathrm{Re}(\lambda(k)) = 0$ at $k = k_\mathrm{c} \neq 0$.[56,58] Then the Turing instability of model (4) occurs when

$$\nu_\mathrm{c} = \frac{\left(2\,d_1 R_0 - d_2 R_0 - d_1 + 3\,d_2 - 2\sqrt{{d_1}^2 {R_0}^2 - d_1 d_2 {R_0}^2 - {d_1}^2 R_0 + 2\,d_1 d_2 R_0}\right)(R_0 - 1)}{d_2 R_0 R_\mathrm{d}}, \tag{12}$$

and the wavenumber k_c satisfies

$$k_\mathrm{c}^2 = \frac{(\nu R_0 R_\mathrm{d} - R_0 + 1)(4 d_2 R_0 - d_2 R_0^2 - d_2 \nu R_0 R_\mathrm{d} - d_1 R_0 + d_1 + 3 d_2)}{2\nu d_1 d_2 R_\mathrm{d} R_0^2}. \tag{13}$$

It is easy to know that when $\nu < \nu_\mathrm{c}$, Turing patterns will emerge.

Figure 1 shows the phase diagram obtained from the linear stability analysis with $R_\mathrm{d} = 1.8$, $d_1 = 0.01$, $d_2 = 0.25$ in R_0–ν plane. Turing bifurcation curve ν_c and the critical boundary line of the positive equilibrium condition $\nu^+ = (R_0 - 1)/(R_0 R_\mathrm{d})$ separate the parametric space into three domains. Domain I, lo-

cated above the Turing bifurcation curve, corresponds to the disease-free system. Domain III, below the critical boundary line of the positive equilibrium condition, is a region of no positive equilibrium. Domain II, below the Turing bifurcation curve and above the critical boundary line of the positive equilibrium condition, the corresponding solution of the model is unstable and Turing instability occurs, so Turing patterns emerge. This domain is called the Turing space.

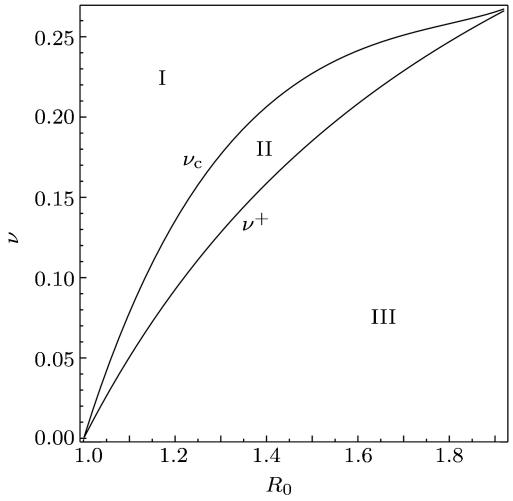


Fig. 1. The phase diagram of model (4) with parameters $R_d = 1.8$, $d_1 = 0.01$, $d_2 = 0.25$. The Turing bifurcation curve ν_c and the critical boundary line $\nu^+ = (R_0 - 1)/(R_0 R_d)$ of the positive equilibrium condition (8) separate the parametric space into three domains. Domain II is called Turing space.

For the sake of further finding the effect of diffusion on the stability of the solutions of model (4), in Fig. 2, we give the relation between Re(λ) and ν. In Fig. 2(a), for model (3) with parameters $R_d = 1.8$, $R_0 = 1.17$, i.e., without diffusion, one can see that the real part of λ is always negative, so the solutions of Eq. (3) are stable. While in Fig. 2(b), for model (4) with $R_d = 1.8$, $R_0 = 1.17$, $d_1 = 0.01$, $d_2 = 0.25$, i.e., with diffusion, it is easy to see that the real part of λ is positive when $0.08072174739 = \nu_1 < \nu < \nu_2 = 0.1200987009$. That is to say, with the fixed parameters, if $\nu_1 < \nu < \nu_2$, the solutions of Eq. (4) are unstable. In this region, despite that the solutions are unstable, the diffusion can de-stabilize the symmetric solutions so that the system with diffusion added can have the symmetry-breaking capabilities, i.e., form the Turing pattern.

From the linear stability analysis, we can obtain the Turing instability for model (4) and determine the conditions of emergency of Turing pattern. Unfortunately, we cannot determine the selection and competition of Turing pattern. In the next section, we shall consider the selection and the formation of Turing patterns close to the onset $\nu = \nu_c$, Turing bifurcation, defined by Eq. (12).

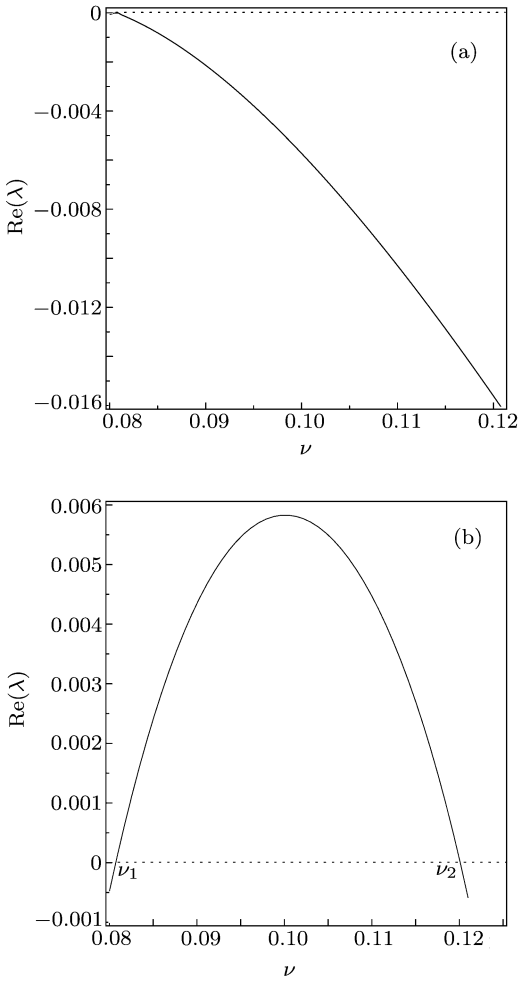


Fig. 2. The relation between Re(λ) and ν. (a) Model (3) with $R_d = 1.8$, $R_0 = 1.17$, Re(λ) < 0, the solutions of Eq. (3) are stable. (b) Model (4) with $R_d = 1.8$, $R_0 = 1.17$, $d_1 = 0.01$, $d_2 = 0.25$ and $\nu_1 = 0.08072174739$, $\nu_2 = 0.1200987009$. In the range $\nu_1 < \nu < \nu_2$, Re(λ) > 0; in this region, the solutions of Eq. (4) are unstable.

3. Pattern formation

3.1. Amplitude equations

A multiple-scale perturbation analysis yields the well-known amplitude equations.[41] And the method of multiple-scale perturbation analysis is based on the fact that near the instability threshold the basic state is unstable only in regard to perturbations with wave numbers close to the critical value, k_c (defined by Eq. (13)). Turing patterns (e.g., hexagonal and stripe patterns) are thus well described by a system of three active resonant pairs of modes $(\boldsymbol{k}_j, -\boldsymbol{k}_j)$ $(j = 1, 2, 3)$ making angles of $2\pi/3$.

Close to onset $\nu = \nu_{\rm c}$, the solutions of Eq. (4) can be expanded as

$$\boldsymbol{U} = \begin{pmatrix} S \\ I \end{pmatrix} = \boldsymbol{U}^* \cdot \sum_{j=1}^{3} \left[A_j \exp(\mathrm{i}\boldsymbol{k}_j \cdot \boldsymbol{r}) + \overline{A}_j \exp(-\mathrm{i}\boldsymbol{k}_j \cdot \boldsymbol{r}) \right], \tag{14}$$

where

$$\boldsymbol{U}^* = \left(\frac{d_1(R_0-1) - \sqrt{d_1 d_2 R_0(2-R_0) + {d_1}^2 R_0(R_0-1)}}{d_2(R_0-1)}, 1 \right)^{\rm T}$$

defines the direction of the eigenmodes (i.e., the ratio S/I) in concentration space; A_j and the conjugate $\overline{A}_j$ are, respectively, the amplitudes associated with modes $\boldsymbol{k}_j$ and $-\boldsymbol{k}_j$, $|k_j| = k_{\rm c}$. By the analysis of the symmetries, up to the third order in the perturbations, the spatiotemporal evolutions of the amplitudes A_j $(j = 1, 2, 3)$ are described through the amplitude equations

$$\begin{cases} \tau_0 \dfrac{\partial A_1}{\partial t} = \mu A_1 + \Gamma \overline{A}_2 \overline{A}_3 - \left[g_1 |A_1|^2 + g_2 (|A_2|^2 + |A_3|^2) \right] A_1, \\ \tau_0 \dfrac{\partial A_2}{\partial t} = \mu A_2 + \Gamma \overline{A}_1 \overline{A}_3 - \left[g_1 |A_2|^2 + g_2 (|A_1|^2 + |A_3|^2) \right] A_2, \\ \tau_0 \dfrac{\partial A_3}{\partial t} = \mu A_3 + \Gamma \overline{A}_1 \overline{A}_2 - \left[g_1 |A_3|^2 + g_2 (|A_1|^2 + |A_2|^2) \right] A_3, \end{cases} \tag{15}$$

where $\mu = (\nu_{\rm c} - \nu)/\nu$ is a normalized distance to onset. Notably, for model (4), the stationary state becomes Turing unstable when the bifurcation parameter ν decreases, so that μ, the distance to onset, increases when the bifurcation parameter ν decreases.

Amplitude equation (15) allows us to study the existence and stability of arrays of hexagons and strips. Close to onset $\nu = \nu_{\rm c}$, the uniform state is unstable only to perturbations with wave vectors close to $k_{\rm c}$ (Eq. (13)). To solve the coefficients of Eqs. (15), we perturb model (4) at the equilibrium (S^*, I^*). Model (4) can be written as

$$\frac{\partial}{\partial t}\boldsymbol{U} = \boldsymbol{L} \cdot \boldsymbol{U} + \boldsymbol{H}, \tag{16}$$

where $\boldsymbol{L}$ is the linear operator, $\boldsymbol{H}$ is the nonlinear terms,

$$\boldsymbol{L} = \begin{bmatrix} f_S + d_1 \boldsymbol{\nabla}^2 & f_I \\ g_S & g_I + d_2 \boldsymbol{\nabla}^2 \end{bmatrix}, \quad \boldsymbol{H} = \begin{bmatrix} H_1 \\ H_2 \end{bmatrix}, \tag{17}$$

where

$$\begin{aligned} H_1 &= \nu R_{\rm d} \Big(2(S+I)^3 - S^2 - I^2 - 2SI \Big) + R_0 SI, \\ H_2 &= I^2 - (R_0 - 1) SI. \end{aligned} \tag{18}$$

The variations of A_i in Eq. (15) occur on a scale much larger than the basic scale and A_i can be written in terms of the slow variables. Near the Turing bifurcation threshold, we expand the bifurcation parameter ν in different orders of ε, $|\varepsilon| \ll 1$,

$$\nu_{\rm c} - \nu = \varepsilon \nu_1 + \varepsilon^2 \nu_2 + \varepsilon^3 \nu_3 + o(\varepsilon^4). \tag{19}$$

Equally,

$$\boldsymbol{U} = \varepsilon \boldsymbol{U}_1 + \varepsilon^2 \boldsymbol{U}_2 + \varepsilon^3 \boldsymbol{U}_3 + o(\varepsilon^4), \tag{20}$$

$$\boldsymbol{H} = \varepsilon^2 \boldsymbol{h}_2 + \varepsilon^3 \boldsymbol{h}_3 + o(\varepsilon^4), \tag{21}$$

$$\begin{aligned} \boldsymbol{L} &= \boldsymbol{L}_{\rm c} + (\nu_{\rm c} - \nu)\boldsymbol{L}_1 + (\nu_{\rm c} - \nu)^2 \boldsymbol{L}_2 + o((\nu_{\rm c} - \nu)^3) \\ &= \boldsymbol{L}_{\rm c} + (\nu_{\rm c} - \nu)\boldsymbol{M} + o((\nu_{\rm c} - \nu)^2), \end{aligned} \tag{22}$$

where

$$\boldsymbol{L}_i = \frac{1}{i!} \frac{\partial^i \boldsymbol{L}}{\partial \nu^i}, \quad \boldsymbol{L}_{\rm c} = \boldsymbol{L}_{(\nu = \nu_{\rm c})}, \quad \boldsymbol{M} = \begin{bmatrix} 0 & 1 \\ 0 & 0 \end{bmatrix}. \tag{23}$$

From the chain rule for differentiation we therefore must make the replacements

$$\frac{\partial}{\partial t} = \varepsilon \frac{\partial}{\partial T_1} + \varepsilon^2 \frac{\partial}{\partial T_2} + o(\varepsilon^3), \tag{24}$$

where $T_1 = \varepsilon t$, $T_2 = \varepsilon^2 t$.

Using scalings (19)–(24), we can expand equation Eq. (16) into a perturbation series with respect to ε.

For order ε^1, we have the following linear equation:

$$\boldsymbol{L}_{\rm c} \boldsymbol{U}_1 = 0. \tag{25}$$

Solving Eq. (25), we obtain

$$\boldsymbol{U}_1 = \boldsymbol{U}_0 \left(\sum_{j=1}^{3} A_j \exp(\mathrm{i}\boldsymbol{k}_j \cdot \boldsymbol{r}) + \text{c.c.} \right), \tag{26}$$

where c.c. denotes the complex conjugate. $\boldsymbol{U}_0$ is the eigenvector of the linear operation $\boldsymbol{L}_{\rm c}$.

For order ε^2, we have

$$\boldsymbol{L}_{\rm c}\boldsymbol{U}_2 = \frac{\partial}{\partial T_1}\boldsymbol{U}_1 - \nu_1 \boldsymbol{M}\boldsymbol{U}_1 - \boldsymbol{h}_2, \tag{27}$$

where $\boldsymbol{h}_2$ represents the terms of order ε^2 in nonlinear expansion $\boldsymbol{H}$. In order to let $\boldsymbol{U}_2$ be nonsingular, the right-hand side of Eq. (27) cannot have a projection on the operator $\boldsymbol{L}_{\rm T}^{\dagger}$ (the Fredholm alternative). This statement leads to the value of $\frac{\partial}{\partial T_1}W_j$ $(j = 1, 2, 3)$. After substituting Eq. (26) into Eq. (27), we can obtain

$$\boldsymbol{U}_2 = \boldsymbol{V}_0 + \Bigg(\sum_{j=1}^{3} \boldsymbol{V}_j \exp(\mathrm{i}\boldsymbol{k}_j \cdot \boldsymbol{r}) + \sum_{j=1}^{3} \boldsymbol{V}_{jj} \exp(2\mathrm{i}\boldsymbol{k}_j \cdot \boldsymbol{r}) + \sum_{j,k=1}^{3} \boldsymbol{V}_{jk} \exp(\mathrm{i}(\boldsymbol{k}_j - \boldsymbol{k}_k) \cdot \boldsymbol{r}) + \text{c.c.} \Bigg), \tag{28}$$

where the vectors $\boldsymbol{V}_0$, $\boldsymbol{V}_j$, $\boldsymbol{V}_{jj}$ and $\boldsymbol{V}_{jk}$ are the coefficients of e, $\mathrm{e}^{\mathrm{i}\boldsymbol{k}_j\cdot\boldsymbol{r}}$, $\mathrm{e}^{2\mathrm{i}\boldsymbol{k}_j\cdot\boldsymbol{r}}$, $\mathrm{e}^{\mathrm{i}(\boldsymbol{k}_j-\boldsymbol{k}_k)\cdot\boldsymbol{r}}$, respectively; they can be solved from Eq. (27).

For order ε^3 in the expansion, we obtain

$$\boldsymbol{L}_{\rm c}\boldsymbol{U}_3 = \frac{\partial}{\partial T_1}\boldsymbol{U}_1 + \frac{\partial}{\partial T_2}\boldsymbol{U}_2 - \nu_1 \boldsymbol{M}\boldsymbol{U}_2 - \nu_2 \boldsymbol{M}\boldsymbol{U}_1 - \boldsymbol{h}_3, \tag{29}$$

where $\boldsymbol{h}_3$ is the terms at order ε^3 in nonlinear terms $\boldsymbol{H}$. After substituting Eqs. (26) and (28) into Eq. (29) and using the Fredholm alternative of order ε^3, we can obtain the values of $\frac{\partial}{\partial T_1}V_j + \frac{\partial}{\partial T_2}W_j$ $(j = 1, 2, 3)$.

The amplitude function A_1 of the basic pattern $\mathrm{e}^{\mathrm{i}\boldsymbol{k}_j\cdot\boldsymbol{r}}$ can be written as

$$\frac{\partial A_1}{\partial t} = \varepsilon \frac{\partial W_1}{\partial t} + \varepsilon^2 \frac{\partial V_1}{\partial t} + o(\varepsilon^4). \tag{30}$$

Substituting the values of $\frac{\partial}{\partial T_1}W_j$ $(j = 1, 2, 3)$ and $\frac{\partial}{\partial T_1}V_j + \frac{\partial}{\partial T_2}W_j$ $(j = 1, 2, 3)$ into Eq. (30) and consider Eq. (24), we obtain the coefficients τ_0, Γ, g_1 and g_2 of amplitude equation (15). In the software Maple, we can obtain the exact but complex expressions of the coefficients τ_0, Γ, g_1 and g_2. The expressions of these coefficients are shown in Appendix A.

With fixed parameters set

$$(R_{\rm d},\, R_0,\, d_1,\, d_2) = (1.8,\, 1.17,\, 0.01,\, 0.25), \tag{31}$$

from the above computation, one can obtain

$$\Gamma = 33.08803180, \quad g_1 = 190.9741185, \quad g_2 = 3888.227316. \tag{32}$$

3.2. Amplitude stability

Each amplitude in Eq. (15) can decompose to mode $\rho_i = |A_i|$ and the corresponding phase angle φ_i. Then, substituting $A_j = \rho_j \exp\varphi_j$ $(j = 1, 2, 3)$ into Eq. (15) and separate the real and imaginary parts, one can obtain four real variable differential equations as follows:

$$\begin{cases} \tau_0 \dfrac{\partial \varphi}{\partial t} = -\Gamma \dfrac{\rho_1^2\rho_2^2 + \rho_1^2\rho_3^2 + \rho_2^2\rho_3^2}{\rho_1\rho_2\rho_3} \sin\varphi, \\ \tau_0 \dfrac{\partial \rho_1}{\partial t} = \mu\rho_1 + \Gamma\rho_2\rho_3\cos\varphi - g_1\rho_1^3 - g_2(\rho_2^2 + \rho_3^2)\rho_1, \\ \tau_0 \dfrac{\partial \rho_2}{\partial t} = \mu\rho_2 + \Gamma\rho_1\rho_3\cos\varphi - g_1\rho_2^3 - g_2(\rho_1^2 + \rho_3^2)\rho_2, \\ \tau_0 \dfrac{\partial \rho_3}{\partial t} = \mu\rho_3 + \Gamma\rho_1\rho_2\cos\varphi - g_1\rho_3^3 - g_2(\rho_1^2 + \rho_2^2)\rho_3, \end{cases} \tag{33}$$

where $\varphi = \varphi_1 + \varphi_2 + \varphi_3$.

The dynamical system (33) possesses four kinds of solutions.[47,61]

(i) The conductive state (O) is given by

$$\rho_1 = \rho_2 = \rho_3 = 0. \tag{34}$$

(ii) Stripes (S) are given by

$$\rho_1 = \sqrt{\frac{\mu}{g_1}} \neq 0, \quad \rho_2 = \rho_3 = 0. \tag{35}$$

(iii) Hexagons $(H_0,\, H_\pi)$ are given by

$$\rho_1 = \rho_2 = \rho_3 = \frac{|\Gamma| \pm \sqrt{\Gamma^2 + 4(g_1 + 2g_2)\mu}}{2(g_1 + 2g_2)}, \tag{36}$$

with $\varphi = 0$ or π and exist for

$$\mu > \mu_1 = \frac{-\Gamma^2}{4(g_1 + 2g_2)}. \tag{37}$$

(iv) The mixed states are given by

$$\rho_1 = \frac{|\Gamma|}{g_2 - g_1}, \quad \rho_2 = \rho_3 = \sqrt{\frac{\mu - g_1\rho_1^2}{g_1 + g_2}}, \tag{38}$$

with $g_2 > g_1$.

In what follows, we will give a discussion about the stability of the above four stationary solutions.

In the case of stripes, to study the stability of stationary solution (35), we give a perturbation at stationary solution $(\rho_0, 0, 0)$, where $\rho_0 = \sqrt{\mu/g_1}$. Setting $\rho_1 = \boldsymbol{\rho}_0 + \Delta\rho_1$, $\rho_2 = \Delta\rho_2$, $\rho_3 = \Delta\rho_3$, linearization of Eq. (33) can be written as

$$\frac{\partial \boldsymbol{\rho}}{\partial t} = \boldsymbol{L}_A \cdot \boldsymbol{\rho}, \tag{39}$$

where

$$\boldsymbol{L}_A = \begin{bmatrix} \mu - 3g_1\rho_0^2 & 0 & 0 \\ 0 & \mu - g_2\rho_0^2 & \Gamma\rho_0 \\ 0 & \Gamma\rho_0 & \mu - g_2\rho_0^2 \end{bmatrix}, \ \boldsymbol{\rho} = \begin{bmatrix} \Delta\rho_1 \\ \Delta\rho_2 \\ \Delta\rho_3 \end{bmatrix}. \tag{40}$$

The characteristic equation of matrix $\boldsymbol{L}_A$ can be obtained as

$$\lambda^3 + P_1\lambda^2 + P_2\lambda + P_3 = 0, \tag{41}$$

where

$$\begin{aligned} P_1 =& \ (3\,g_1 + 2\,g_2)\,{\rho_0}^2 - 3\,\mu, \\ P_2 =& \ \left(6\,g_1\,g_2 + {g_2}^2\right){\rho_0}^4 - \left(4\,\mu\,g_2 + \Gamma^2 + 6\,\mu\,g_1\right){\rho_0}^2 \\ & + 3\,\mu^2, \\ P_3 =& \ 3\,g_1\,{g_2}^2\,{\rho_0}^6 - \left(3\,g_1\,\Gamma^2 + \mu\,{g_2}^2 + 6\,\mu\,g_1\,g_2\right){\rho_0}^4 \\ & + \left(2\,\mu^2 g_2 + 3\,g_1\,\mu^2 + \mu\,\Gamma^2\right){\rho_0}^2 - \mu^3. \end{aligned}$$

The eigenvalues of characteristic equation (41) are solved as

$$\begin{aligned} &\lambda_1 = \mu - 3\,g_1\,{\rho_0}^2, \quad \lambda_2 = \mu + \Gamma\rho_0 - g_2\,{\rho_0}^2, \\ &\lambda_3 = \mu - \Gamma\rho_0 - g_2\,{\rho_0}^2. \end{aligned} \tag{42}$$

Substituting $\rho_0 = \sqrt{\mu/g_1}$ into Eq. (42), we obtain

$$\begin{aligned} &\lambda_1 = -2\mu, \quad \lambda_2 = \mu(1 - g_2/g_1) + \Gamma\sqrt{\mu/g_1}, \\ &\lambda_3 = \mu(1 - g_2/g_1) - \Gamma\sqrt{\mu/g_1}. \end{aligned} \tag{43}$$

It is easy to know that equation (33) has stable solutions when the eigenvalues λ_1, λ_2 and λ_3 are all negative. Since in Eq. (33), $\mu > 0$, $g_2/g_1 > 1$, these three eigenvalues are negative if the following condition holds:

$$\mu > \mu_3 = \frac{\Gamma^2 g_1}{(g_2 - g_1)^2}. \tag{44}$$

Next, we consider the stability of the hexagons. Similar to the above process, we perturb Eq. (33) at the point (ρ_0, ρ_0, ρ_0) as follows:

$$\rho_i = \rho_0 + \Delta\rho_i, \quad i = 1, 2, 3, \tag{45}$$

where $\rho_0 = \dfrac{|\Gamma| \pm \sqrt{\Gamma^2 + 4(g_1 + 2g_2)\mu}}{2(g_1 + 2g_2)}$. Under the perturbation, equation (33) can be linearized as

$$\frac{\partial\boldsymbol{\rho}}{\partial t} = \boldsymbol{L}_B \cdot \boldsymbol{\rho}, \tag{46}$$

and

$$\boldsymbol{L}_B = \begin{bmatrix} \mu - (3\,g_1 + 2\,g_2)\,{\rho_0}^2 & \Gamma\rho_0 - 2\,g_2\,{\rho_0}^2 & \Gamma\rho_0 - 2\,g_2\,{\rho_0}^2 \\ \Gamma\rho_0 - 2\,g_2\,{\rho_0}^2 & \mu - (3\,g_1 + 2\,g_2)\,{\rho_0}^2 & \Gamma\rho_0 - 2\,g_2\,{\rho_0}^2 \\ \Gamma\rho_0 - 2\,g_2\,{\rho_0}^2 & \Gamma\rho_0 - 2\,g_2\,{\rho_0}^2 & \mu - (3\,g_1 + 2\,g_2)\,{\rho_0}^2 \end{bmatrix}, \quad \boldsymbol{\rho} = \begin{bmatrix} \Delta\rho_1 \\ \Delta\rho_2 \\ \Delta\rho_3 \end{bmatrix}. \tag{47}$$

The characteristic equation of $\boldsymbol{L}_B$ can be obtained as

$$\lambda^3 + Q_1\lambda^2 + Q_2\lambda + Q_3 = 0, \tag{48}$$

where

$$\begin{aligned} Q_1 =& \ (9\,g_1 + 6\,g_2)\,{\rho_0}^2 - 3\,\mu, \\ Q_2 =& \ \left(27\,{g_1}^2 + 36\,g_1\,g_2\right){\rho_0}^4 + 12\,\Gamma{\rho_0}^3 g_2 \\ & - \left(18\,\mu\,g_1 + 3\,\Gamma^2 + 12\,\mu\,g_2\right){\rho_0}^2 + 3\,\mu^2, \\ Q_3 =& \ \left(54\,{g_1}^2 g_2 + 27\,{g_1}^3\right){\rho_0}^6 + 36\,g_1\,\Gamma g_2{\rho_0}^5 \\ & + (6\,g_2\,\Gamma^2 - 36\,\mu\,g_1\,g_2 - 9\,g_1\,\Gamma^2 - 27\,\mu\,{g_1}^2){\rho_0}^4 \\ & - \left(2\,\Gamma^3 + 12\,\mu\,\Gamma g_2\right){\rho_0}^3 \\ & + \left(9\,\mu^2 g_1 + 6\,\mu^2 g_2 + 3\,\mu\,\Gamma^2\right){\rho_0}^2 - \mu^3. \end{aligned}$$

Solving the characteristic equation (48), we can obtain the eigenvalues

$$\begin{aligned} &\lambda_1 = \lambda_2 = \mu - \Gamma\rho_0 - 3\,g_1\,{\rho_0}^2, \\ &\lambda_3 = \mu - 3\,g_1\,{\rho_0}^2 - 6\,g_2\,{\rho_0}^2 + 2\,\Gamma\rho_0. \end{aligned} \tag{49}$$

Substituting the stationary hexagon solution (36) into Eq. (49), we can obtain two cases of stability as follows.

For the stationary solution

$$\rho_0^- = \frac{|\Gamma| - \sqrt{\Gamma^2 - 4(g_1 + 2g_2)\mu}}{2(g_1 + 2g_2)},$$

λ_1 and λ_2 are always positive, so the corresponding pattern is also always unstable.

For the stationary solution

$$\rho_0^+ = \frac{|\Gamma| + \sqrt{\Gamma^2 + 4(g_1 + 2g_2)\mu}}{2(g_1 + 2g_2)},$$

$\lambda_i\,(i = 1, 2, 3)$ is negative when the parameter μ satisfies the following condition:

$$\mu < \mu_4 = \frac{2g_1 + g_2}{(g_2 - g_1)^2}h^2. \tag{50}$$

Summarize the above analyses, we can conclude

(I) The conductive state (O) is stable for $\mu < \mu_2 = 0$ and unstable for $\mu > \mu_2$.

(II) The stripe is stable when $\mu > \mu_3 = \frac{\Gamma^2 g_1}{(g_2-g_1)^2}$.

(III) The hexagon H_0 is stable only for $\mu < \mu_4 = \frac{2g_1+g_2}{(g_2-g_1)^2}\Gamma^2$ and hexagon H_π is always unstable.

(IV) the mixed states can exist for $\mu > \mu_3$ and are always unstable.

With fixed parameter set (31), one can obtain

$$\mu_1 = -0.06409677030, \qquad \mu_2 = 0,$$
$$\mu_3 = 0.3114118460, \quad \mu_4 = 0.6381189919. \quad (51)$$

The existence and stability limits of the solutions, as functions of the scaled bifurcation parameter μ, are ordered according to the scheme in Fig. 3. Stable branches H_0 and H_π are mutually exclusive. With the parameters set (31), the stable branch is H_0 because $\Gamma = 33.08803180 > 0$. A subcritical hexagonal branch comes out first at $\mu > \mu_1 = -0.06409677030$, but loses stability when $\mu > \mu_4 = 0.6381189919$. The supercritical stripe state branch S is unstable when close to the critical point but becomes stable for $\mu > \mu_3 = 0.3114118460$. In the range $\mu_3 < \mu < \mu_4$, both branches H_0 and S are stable.

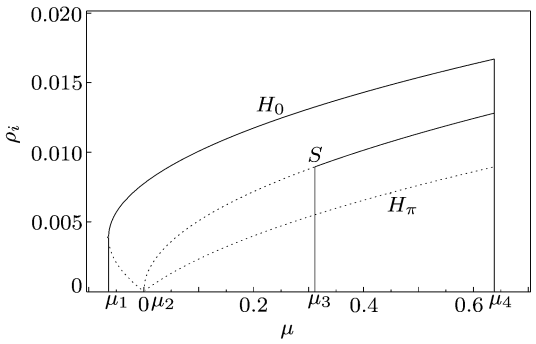


Fig. 3. Bifurcation diagram for model (2) with parameters $R_d = 1.8$, $R_0 = 1.17$, $d_1 = 0.01$, $d_2 = 0.25$. H_0: hexagonal patterns with $\varphi = 0$; H_π: hexagonal patterns with $\varphi = \pi$; S: stripe patterns. The solid lines and dotted lines represent stable states and unstable states respectively. $\mu_1 = -0.06409677030$ (corresponding to $\nu = 0.1283238449$), $\mu_2 = 0$ ($\nu = 0.1200987009$), $\mu_3 = 0.3114118460$ ($\nu = 0.08269854275$), $\mu_4 = 0.6381189919$ ($\nu = 0.04346143895$).

3.3. Pattern selection

In this subsection, we perform extensive numerical simulations of the spatially extended model (4) in 2-dimensional (2D) spaces, and the qualitative results are shown here. All our numerical simulations employ the non-zero initial and zero-flux boundary conditions (i.e., Eqs. (5) and (6)) with a system size of $L\times L$, with $L = 100$ discretized through $x \to (x_0, x_1, x_2, \cdots, x_N)$ and $y \to (y_0, y_1, y_2, \cdots, y_N)$, with $N = 300$. The time steps $\tau = 0.1$, other parameters are fixed as in expression (31).

We use the standard five-point approximation for the 2D Laplacian with the zero-flux boundary conditions.[62] More precisely, the concentrations $(S^{n+1}_{i,j}, I^{n+1}_{i,j})$ at the moment $(n+1)\tau$ at the mesh position (x_i, y_j) are given by

$$S^{n+1}_{i,j} = S^n_{i,j} + \tau d_1 \Delta_h S^n_{i,j} + \tau f(S^n_{i,j}, I^n_{i,j}),$$
$$I^{n+1}_{i,j} = I^n_{i,j} + \tau d_2 \Delta_h I^n_{i,j} + \tau g(S^n_{i,j}, I^n_{i,j}),$$

with the Laplacian defined by

$$\Delta_h S^n_{i,j} = \frac{S^n_{i+1,j} + S^n_{i-1,j} + S^n_{i,j+1} + S^n_{i,j-1} - 4S^n_{i,j}}{h^2},$$

where $h = \frac{L}{N} = \frac{1}{3}$, $f(S, I)$ and $g(S, I)$ are defined in Eq. (4).

Initially, the entire system is placed in the stationary state (S^*, I^*) and the propagation velocity of the initial perturbation is thus on the order of 5×10^{-4} space units per time unit. And the system is then integrated for 10^5 or 10^6 time steps and some images are saved. After the initial period during which the perturbation spreads, the system either goes into a time-dependent state, or to an essentially steady state (time independent).

In the numerical simulations, different types of dynamics are observed and we have found that the distributions of susceptible and infected species are always of the same type. Consequently, we can restrict our analysis of pattern formation to one distribution. In this section, we show the distribution of susceptible S for instance.

When the parameter is located in domain II in Fig. 1, the so-called Turing space, the model dynamics exhibits spatiotemporal complexity of Turing pattern formation. In Fig.4, via numerical simulation, we show typical stationary snapshots arising from random initial conditions for several values of ν or μ.

In Fig. 4(a), H_π-pattern, $\mu_2 < \mu = 0.0174748010$ (corresponding to $\nu = 0.118$), it consists of black (minimum density of S) hexagons on a white (maximum density of S) background, i.e., isolated zones with low population density. We call this pattern holes. In this case, the infectious are isolated zones with high

population density, that means, the epidemic may be outbreak in the region.

In Fig. 4(b), when increasing μ to 0.0341277705 ($\nu = 0.116$), a few of stripes emerge and the remainder of the holes pattern remains time independent, i.e., it is a stripes–holes pattern. This pattern is called H_π-hexagon-stripe mixture pattern, when increasing μ to 0.0591072247 ($\nu = 0.113$), model dynamics exhibits a transition from stripes–holes growth to stripes replication, i.e., holes decay and the stripes pattern emerges (Fig. 4(c)).

In Fig. 4(d), $\mu = 0.1506985568$ ($\nu = 0.102$), with increasing μ, a few of white hexagons (i.e., spots, associated with high population densities) fill in the stripes, i.e., the stripes–spots pattern emerges. This pattern is called H_0-hexagon-stripe mixture pattern, when increasing μ to $0.3172282516 > \mu_3 = 0.3114124327$ ($\nu = 0.082$), model dynamics exhibits a transition from stripe–spot growth to spots replication, i.e., stripes decay and the spots pattern (H_0-pattern) emerges (Fig. 4(e)). Under the control of these parameters, the infectious are isolated in zones with low population density, that means the epidemic may not outbreak in the region. In other words, in this case, the region is safe.

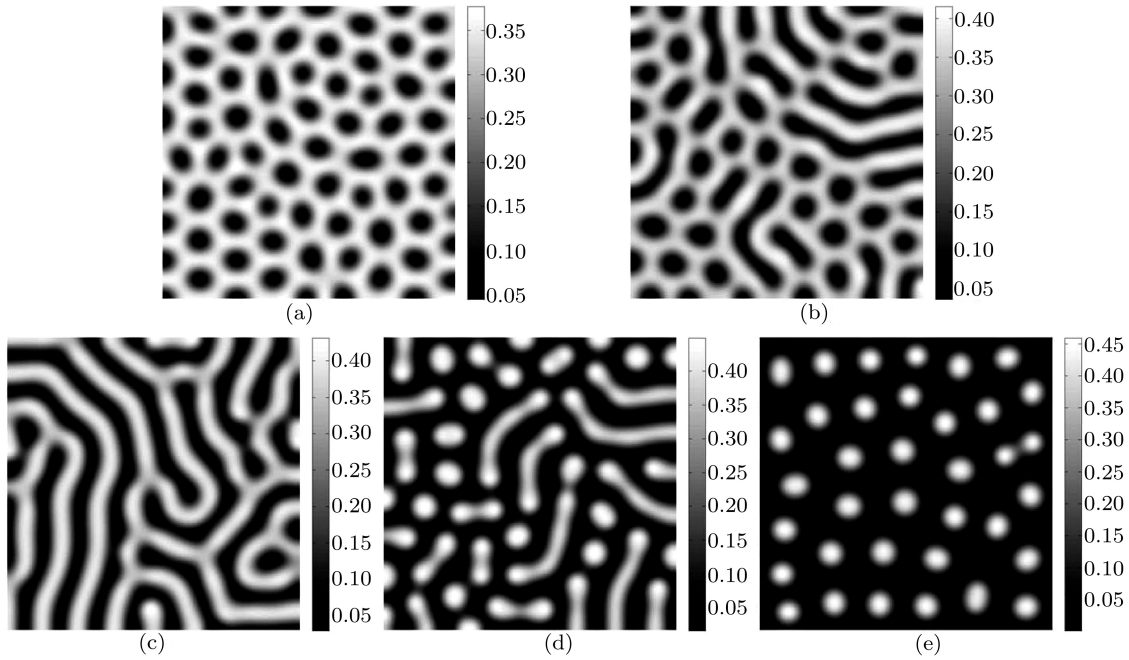


Fig. 4. Five categories of Turing patterns of S in model (4) with parameters $R_\mathrm{d} = 1.8$, $R_0 = 1.17$, $d_1 = 0.01$, $d_2 = 0.25$. (a) $\mu = 0.017474801$ ($\nu = 0.118$); (b) $\mu = 0.0341277705$ ($\nu = 0.116$); (c) $\mu = 0.0591072247$ ($\nu = 0.113$); (d) $\mu = 0.1506985568$ ($\nu = 0.102$); (e) $\mu = 0.3172282516$ ($\nu = 0.082$). The iteration numbers are (a), (e) 200000; (b), (c), (d) 100000.

From Fig. 4, one can see that values for the concentration S are represented in a grey scale varying from black (minimum) to white (maximum). On increasing the control parameter μ, the sequence H_π hexagons $\rightarrow$ H_π-hexagon-stripe mixtures $\rightarrow$ stripes $\rightarrow$ H_0-hexagon-stripe mixtures $\rightarrow$ H_0-hexagons can be observed. Notably, in these cases, the distance to onset (i.e., μ) decreases when ν increases. That is to say, on increasing the control parameter ν, the sequence H_0 hexagons $\rightarrow$ H_0-hexagon-stripe mixtures $\rightarrow$ stripes $\rightarrow$ H_π-hexagon-stripe mixtures $\rightarrow$ H_π hexagons is observed.

4. Conclusions and remarks

In summary, this study presents the Turing pattern selection in a spatial epidemic model. The value of this study is twofold. First, it establishes the amplitude equations for the excited modes, which determines the stability of amplitudes towards uniform and inhomogeneous perturbations. Second, it illustrates all five categories of Turing patterns close to the onset of Turing bifurcation via numerical simulations which indicates that the model dynamics exhibits complex pattern replication.

In the epidemic model (1) or (4), with the

fixed parameters $R_{\rm d} = 1.8, R_0 = 1.17$, for obtaining the positive equilibrium, from condition (8), we know $\nu > 0.08072174739$, which corresponds to $\mu = 0.3278716024$. That is to say, for model (4), the normalized distance to onset is $\mu < 0.3278716024$. On the other hand, from the results of Fig. 1 and Eq. (51), one can know that with the fixed parameters set (31), when $\nu > 0.1200987009$ (corresponding to $\mu = 0$), i.e., parameters located in the domain I in Fig. 1, the steady state is only the stable solution of model (4). Briefly, $0 < \mu < 0.3278716024$ (i.e., $0.08072174739 < \nu < 0.1200987009$), there exhibits the emergency of Turing patterns (domain II in Fig. 2).

In contrast to the results in Refs. [33] and [36–38], we find that the spatial epidemic model dynamics exhibits a diffusion-controlled formation growth not only to stripes and stripes–spots but also to holes, stripes–holes and spots replication. That is to say, the pattern formation of the epidemic model is not simple, but richer and complex.

The methods and results in the present paper may enrich the research of the pattern formation in the spatial epidemic model, or may be useful for other reaction–diffusion systems.

Appendix A: The coefficients of the amplitude Eq. (15)

Set

$$Q = \sqrt{d_1 R_0\,(d_1 R_0 - d_2 R_0 + 2\,d_2 - d_1)},$$

then the coefficients of the amplitude equations (15) are obtained as follows:

$$\tau_0 = \frac{A_1}{A_2}, \tag{A1}$$

$$\begin{aligned}
A_1 &= R_0(d_2 R_0 - 2\,d_1 R_0 - 3\,d_2 + d_1 + 2\,Q)\,(d_1 - d_1 R_0 + Q)(d_1 - d_2),\\
A_2 &= (12\,{d_1}^2 d_2 - 8\,{d_1}^3 - 4\,d_1 {d_2}^2){R_0}^4 + (-46\,{d_1}^2 d_2 + 20\,{d_1}^3 - 8\,Q d_1 d_2 + 8\,Q {d_1}^2 + 22\,d_1 {d_2}^2\\
&\quad + {d_2}^2 Q){R_0}^3 + (52\,{d_1}^2 d_2 + 28\,Q d_1 d_2 - 38\,d_1 {d_2}^2 - 16\,{d_1}^3 - 6\,{d_2}^2 Q - 16\,Q {d_1}^2){R_0}^2\\
&\quad + (9\,Q {d_1}^2 - 18\,{d_1}^2 d_2 + 11\,{d_2}^2 Q + 20\,d_1 {d_2}^2 + 4\,{d_1}^3 - 25\,Q d_1 d_2) R_0 - Q {d_1}^2 + 5\,Q d_1 d_2 - 6\,{d_2}^2 Q.
\end{aligned}$$

$$\Gamma = \frac{A_3}{A_4}, \tag{A2}$$

$$\begin{aligned}
A_3 &= 2\,R_0\,((d_2 - 2\,d_1)R_0 + 2\,Q - 3\,d_2 + d_1)((8\,d_1 d_2 - 6\,{d_1}^2 - 2\,{d_2}^2){R_0}^2 + (8\,{d_1}^2 - 5\,d_2 Q\\
&\quad + 6\,d_1 Q - 18\,d_1 d_2 + 7\,{d_2}^2) R_0 - 5\,d_1 Q + 7\,d_1 d_2 - 2\,{d_1}^2 + 8\,d_2 Q - 6\,{d_2}^2,\\
A_4 &= (12\,{d_1}^2 d_2 - 4\,d_1 {d_2}^2 - 8\,{d_1}^3){R_0}^4 + (8\,Q {d_1}^2 - 46\,{d_1}^2 d_2 + 20\,{d_1}^3 + 22\,d_1 {d_2}^2 + {d_2}^2 Q\\
&\quad - 8\,d_1 Q d_2){R_0}^3 + (28\,d_1 Q d_2 + 52\,{d_1}^2 d_2 - 38\,d_1 {d_2}^2 - 6\,{d_2}^2 Q - 16\,{d_1}^3 - 16\,Q {d_1}^2){R_0}^2\\
&\quad + (4\,{d_1}^3 + 9\,Q {d_1}^2 - 25\,d_1 Q d_2 - 18\,{d_1}^2 d_2 + 11\,{d_2}^2 Q + 20\,d_1 {d_2}^2) R_0 - Q {d_1}^2 - 6\,{d_2}^2 Q + 5\,d_1 Q d_2.
\end{aligned}$$

$$g_1 = \frac{A_5}{A_6}, \tag{A3}$$

$$\begin{aligned}
A_5 &= R_0\,(d_1 + 2\,Q - 2\,d_1 R_0 - 3\,d_2)(165\,{d_1}^3 {R_0}^2 - 111\,d_1 {R_0}^2 Q d_2 + 221\,Q d_1 R_0\,d_2\\
&\quad + 471\,d_1 {R_0}^2 {d_2}^2 - 497\,{d_1}^2 {R_0}^2 d_2 - 732\,d_1 {d_2}^2 R_0 + 471\,{d_1}^2 d_2 R_0 + 360\,d_1 {d_2}^2 - 192\,{d_1}^2 d_2\\
&\quad - 66\,Q d_1 d_2 - 111\,Q {d_1}^2 R_0 + 108\,Q {d_1}^2 {R_0}^2 + 33\,{d_2}^2 {R_0}^2 Q - 66\,{d_2}^2 R_0\,Q + 32\,{d_2}^3 {R_0}^3\\
&\quad - 192\,{d_2}^3 {R_0}^2 + 32\,{d_1}^3 - 89\,d_1 {R_0}^3 {d_2}^2 - 89\,{d_1}^3 R_0 - 216\,{d_2}^3 + 360\,{d_2}^3 R_0 - 108\,{R_0}^3 {d_1}^3\\
&\quad + 165\,{d_1}^2 {R_0}^3 d_2 + 45\,{d_2}^2 Q + 33\,Q {d_1}^2),
\end{aligned}$$

$$\begin{aligned}
A_6 &= 9\,d_1(12\,{d_1}^3 {R_0}^2 + Q {d_1}^2 + 18\,d_1 {R_0}^2 {d_2}^2 - 34\,{d_1}^2 {R_0}^2 d_2 - 20\,d_1 {d_2}^2 R_0 + 18\,{d_1}^2 d_2 R_0\\
&\quad - 4\,d_1 {R_0}^3 {d_2}^2 - 4\,{d_1}^3 R_0 - 8\,{R_0}^3 {d_1}^3 + 12\,{d_1}^2 {R_0}^3 d_2 + 8\,Q {d_1}^2 {R_0}^2 - 8\,d_1 {R_0}^2 Q d_2 + 20\,Q d_1 R_0\,d_2\\
&\quad - 8\,Q {d_1}^2 R_0 + 6\,{d_2}^2 Q - 5\,{d_2}^2 R_0\,Q + {d_2}^2 {R_0}^2 Q - 5\,Q d_1 d_2)({R_0}^2 - 2\,R_0 + 1).
\end{aligned}$$

$$g_2 = \frac{A_7}{A_8}, \tag{A4}$$

$$\begin{aligned}
A_7 = {} & (12\,{d_2}^3 - 76\,d_1{d_2}^2 - 60\,{d_1}^3 + 124\,{d_1}^2 d_2)(d_2 - 2\,d_1){R_0}^5 + ((36\,{d_2}^2 Q - 382\,{d_1}^2 d_2 + 124\,{d_1}^3 \\
& + 324\,d_1{d_2}^2 - 94\,Qd_1d_2 + 60\,Q{d_1}^2 - 72\,{d_2}^3)(d_2 - 2\,d_1) + (124\,{d_1}^2 d_2 - 76\,d_1{d_2}^2 - 60\,{d_1}^3 \\
& + 12{d_2}^3)(2\,Q - 3\,d_2 + d_1)){R_0}^4 + ((324\,{d_1}^2 d_2 - 76\,{d_1}^3 + 240\,Qd_1d_2 - 94\,Q{d_1}^2 - 408\,d_1{d_2}^2 \\
& + 135\,{d_2}^3 - 129\,{d_2}^2 Q)(d_2 - 2\,d_1) + (36\,{d_2}^2 Q - 382\,{d_1}^2 d_2 + 124\,{d_1}^3 + 324\,d_1{d_2}^2 - 94\,Qd_1d_2 \\
& + 60\,Q{d_1}^2 - 72\,{d_2}^3)(2\,Q - 3\,d_2 + d_1)){R_0}^3 + ((135\,d_1{d_2}^2 - 72\,{d_1}^2 d_2 - 129\,Qd_1d_2 - 81\,{d_2}^3 \\
& + 12\,{d_1}^3 + 117\,{d_2}^2 Q + 36\,Q{d_1}^2)(d_2 - 2\,d_1) + (324\,{d_1}^2 d_2 - 76\,{d_1}^3 + 240\,Qd_1d_2 - 94\,Q{d_1}^2 \\
& - 408\,d_1{d_2}^2 + 135\,{d_2}^3 - 129\,{d_2}^2 Q)(2\,Q - 3\,d_2 + d_1)){R_0}^2 + (+12\,{d_1}^3 - 129\,Qd_1d_2 - 81\,{d_2}^3 \\
& + 135\,d_1{d_2}^2 - 72\,{d_1}^2 d_2 + 117\,{d_2}^2 Q + 36\,Q{d_1}^2)(2\,Q - 3\,d_2 + d_1)R_0.
\end{aligned}$$

$$\begin{aligned}
A_8 = {} & d_1(12\,{d_1}^3 {R_0}^2 + Q{d_1}^2 + 18\,d_1 R_0{}^2 {d_2}^2 - 34\,{d_1}^2 {R_0}^2 d_2 - 20\,d_1{d_2}^2 R_0 + 18\,{d_1}^2 d_2 R_0 - 4\,d_1 {R_0}^3 {d_2}^2 \\
& - 4\,{d_1}^3 R_0 - 8\,{R_0}^3 {d_1}^3 + 12\,{d_1}^2 {R_0}^3 d_2 + 8\,Q{d_1}^2 {R_0}^2 - 8\,d_1 {R_0}^2 Q d_2 + 20\,Qd_1R_0\,d_2 - 8\,Q{d_1}^2 R_0 \\
& + 6\,{d_2}^2 Q - 5\,{d_2}^2 R_0\,Q + {d_2}^2 {R_0}^2 Q - 5\,Qd_1d_2)({R_0}^2 - 2\,R_0 + 1).
\end{aligned}$$

References

[1] Ma Z E, Zhou Y C and Wu J H 2009 *Modeling and Dynamics of Infectious Diseases* (Beijing: Higher Education Press)

[2] Kermack W O and McKendrick A G 1927 *Proc. R. Soc. Lond.* A **115** 700

[3] Hethcote H W 2000 *SIAM Rev.* **42** 599

[4] Fan M, Li Y M and Wang K 2001 *Math. Biosci.* **170** 199

[5] Li Y M, Smith H L and Wang L C 2001 *SIAM J. Appl. Math.* **62** 58

[6] Ruan S G and Wang W D 2003 *J. Differential Equations* **188** 135

[7] Berezovsky F, Karev G, Song B and Castillo-Chavez C 2004 *Math. Biosci. Eng.* **1** 1

[8] Wang W D and Zhao X Q 2004 *Math. Biosci.* **190** 97

[9] Wang W D and Ruan S G 2004 *J. Math. Anal. Appl.* **291** 775

[10] Allen L J S, Bolker B M, Lou Y and Nevai A L 2007 *SIAM J. Appl. Math.* **67** 1283

[11] Xiao D M and Ruan S G 2007 *Math. Biosci.* **208** 419

[12] Jin Z and Liu Q X 2006 *Chin. Phys.* **15** 1248

[13] Zheng Z Z and Wang A L 2009 *Chin. Phys.* B **18** 489

[14] Zhang H F, Michael S, Fu X C and Wang B H 2009 *Chin. Phys.* B **18** 3639

[15] Liu M X and Ruan J 2009 *Chin. Phys.* B **18** 5111

[16] Hosono Y and Ilyas B 1995 *Math. Models Methods Appl. Sci.* **5** 935

[17] Cruickshank I, Gurney W and Veitch A 1999 *Theor. Popu. Biol.* **56** 279

[18] Turechek W W and Madden L V 1999 *Phytopathology* **89** 421

[19] Ferguson N M, Donnelly C A and Anderson R M 2001 *Science* **292** 1155

[20] Grenfell B T, Bjornstad O N and Kappey J 2001 *Nature* **414** 716

[21] Britton N F 2003 *Essential Mathematical Biology* (London: Springer Verlag)

[22] He D H and Stone L 2003 *Proc. R. Soc. Lond.* B **270** 1519

[23] Lloyd A L and Jansen V A 2004 *Math. Biosci.* **188** 1

[24] van Ballegooijen W M and Boerlijst M C 2004 *Proc. Natl. Acad. Sci.* **101** 18246

[25] Filipe J A N and Maule M M 2004 *J. Theor. Biol.* **226** 125

[26] Kenkre V M 2004 *Phys.* A **342** 242

[27] Funk G A, Jansen V A A, Bonhoeffer S and Killingback T 2005 *J. Theor. Biol.* **233** 221

[28] Pascual M and Guichard F 2005 *TREE* **20** 88

[29] Festenberg N V, Gross T and Blasius B 2007 *Math. Model. Nat. Phenom.* **2** 63

[30] Mulone G, Straughan B and Wang W 2007 *Studies in Appl. Math.* **118** 117

[31] Wang K F and Wang W D 2007 *Math. Biosci.* **210** 78

[32] Wang K F, Wang W D and Song S P 2008 *J. Theor. Biol.* **253** 36

[33] Liu Q X and Jin Z 2007 *J. Stat. Mech.* P05002

[34] Malchow H, Petrovskii S V and Venturino E 2008 *Spatiotemporal Patterns in Ecology and Epidemiology–Theory, Models and Simulation* (Boca Raton: Chapman & Hall/CRC)

[35] Xu R and Ma Z E 2009 *J. Theor. Biol.* **257** 499

[36] Sun G Q, Jin Z, Liu Q X and Li L 2008 *J. Stat. Mech.* P08011

[37] Sun G Q, Jin Z, Liu Q X and Li L 2008 *Chin. Phys.* B **17** 3936

[38] Li L, Jin Z and Sun G Q 2008 *Chin. Phys. Lett.* **25** 3500

[39] Turing A M 1952 *Philos. T. Roy. Soc.* B **237** 37

[40] Newell A C and Whitehead J A 1969 *J. Fluid Mech.* **38** 279

[41] Peña B and Pérez-García C 2000 *Europhys. Lett.* **51** 300

[42] Peña B and Pérez-García C 2001 *Phys. Rev.* E **64** 056213

[43] Gunaratne G H, Ouyang Q and Swinney H L 1994 *Phys. Rev.* E **50** 2802

[44] Segel L A 1969 *J. Fluid Mech.* **38** 203

[45] Ipsen M, Hynne F and Sorensen P G 1998 *Chaos* **8** 834

[46] Ipsen M, Hynne F and Sorensen P G 2000 *Physica* D **136** 66

[47] Ouyang Q 2000 *Pattern Formation in Reaction-Diffusion Systems* (Shanghai: Shanghai Sci-Tech Education Publishing House) (in Chinese)
[48] Ouyang Q, Gunaratne G H and Swinney H L 1993 *Chaos* **3** 707
[49] Callahan T K and Knobloch E 1999 *Physica* D **132** 339
[50] Dufiet V and Boissonade J 1992 *J. Chem. Phys.* **96** 664
[51] Dufiet V and Boissonade J 1992 *Phys.* A **188** 158
[52] Dufiet V and Boissonade J 1996 *Phys. Rev.* E **53** 4883
[53] Wang W M, Lin Y Z, Rao F, Zhang L and Tan Y J 2010 *J. Stat. Mech.* P11036
[54] Wang W M, Wang W J, Lin Y Z and Tan Y J 2011 *Chin. Phys.* B **20** 034702
[55] Okubo A and Levin S A 2001 *Diffusion and Ecological Problems: Modern Perspectives* 2nd ed (New York: Springer)
[56] Murray J D 2003 *Mathematical Biology* 3rd ed (New York: Springer)
[57] Baurmann M, Gross T and Feudel U 2007 *J. Theor. Biol.* **245** 220
[58] Wang W M, Liu Q X and Jin Z 2007 *Phys. Rev.* E **75** 051913
[59] Wang W M, Zhang L, Wang H L and Li Z Q 2010 *Ecol. Model.* **221** 131
[60] Lin W 2010 *Chin. Phys.* B **19** 090206
[61] Ciliberto S, Coullet P, Lega J, Pampaloni E and Perez-Garcia C 1990 *Phys. Rev. Lett.* **65** 2370
[62] Munteanu A and Sole R V 2006 *Int. J. Bif. Chaos* **16** 3679